Journal of Microscopy, Vol. 188, Pt 3, December 1997, pp. 273–279.
Received 2 December 1996; accepted 6 June 1997

Axial resolution of confocal Raman microscopes: Gaussian beam theory and practice

C. J. DE GRAUW, N. M. SIJTSEMA, C. OTTO & J. GREVE
Department of Applied Physics, Biomedical Technology Institute, Twente University, PO Box 217, 7500 AE Enschede, The Netherlands

Key words. Confocal microscopy, depth resolution.

Summary

A straightforward and transparent model, based on Gaussian beam optics, for the axial r_0 resolution of a confocal microscope is presented. A confocal Raman microscope was used to determine the axial confocality in practice. The axial response of a thin planar object was measured for three different objectives, two pinhole sizes and a slit. The results show that, in the case of a confocal configuration, the response calculated with the model provides a good prediction of the axial resolution of the confocal microscope.

Introduction

Confocal Raman microscopy is a well-established technique for the investigation of the three-dimensional (3-D) structure of biological samples. It has been applied successfully to lymphocytes and chromosomes (Puppels *et al.*, 1990, 1995) and eye lenses (Duindam *et al.*, 1995) using spontaneous Raman scattering and to K562 cancer cells using microsurface enhanced Raman scattering (Sharonov *et al.*, 1994). In confocal microscopy a microscope objective forms a diffraction-limited image of the laser source in the object. An image of the illuminated object is formed at the position of the fieldstop. The two common types of fieldstop used are a circular pinhole and a rectangular slit. If the size of the fieldstop is equal to or smaller than the image of the object, the set-up is considered to be confocal. The lateral resolution is influenced directly by the fieldstop, which truncates the field of view for the detector. In a confocal microscope the axial resolution is determined by the reduction of the out-of-focus signal. The choice of a slit or pinhole entrance of the detector stage depends on the resolution and signal intensity desired. If a pinhole is chosen to obtain optimal resolution, the signal intensity may be too low. A larger pinhole and consequently lower resolution may then be selected. As a compromise a slit can be chosen (Wilson & Hewlett, 1990).

The confocal principle has been described before (Wilson, 1990) where the 3-D response functions are used to calculate the lateral and axial response of a uniformly illuminated point object, a plane object and a line object for an infinitely small pinhole using a low angular approximation. Using the same approximation the response function has been calculated, with a finite sized pinhole, for a uniformly illuminated point object and for a reflecting plane (Wilson & Carlini, 1987; Wilson & Tan, 1995). In biological samples like cells, chromosomes or tissue the situation is usually considerably more complicated. The specimen is illuminated through a high-magnification objective and examined in reflection by the same objective. The total scattered signal is therefore influenced by the structural details of the object. The dimensions and the differences in refractive index within the specimen and between the specimen and the surrounding medium influence the light collection. Therefore the response coming from a reflecting plane or a point source will not give a correct description of the resolution in such samples. Based on extensive calculations, using electromagnetic diffraction theory, the response of a confocal microscope for high numerical aperture objectives, finite pinhole size and plane objects was determined (van der Voort & Brakenhoff, 1990).

Experimentally, the axial resolution of a confocal microscope can be obtained in various ways. In general, an object is scanned along the optical axis, resulting in a response curve. Two types of object are used: thin planar objects and small particles, typically smaller than the diffraction limit (Fig. 1). Using a thin planar object of strong Raman scattering an axial resolution of 1·8 μm was determined by Markwort *et al.* (1995). Small beads were used by Puppels *et al.* (1991) and Brakenhoff *et al.* (1986) yielding a resolution of 1·3 μm and 1·5 μm, respectively. The exact resolution depends on the excitation wavelength and the numerical aperture of the objective. The axial resolution in these

Correspondence to: C. Otto; tel: +31–53–4893157; fax: +31 53 4891105; E-mail: c.otto@tn.utwente.nl

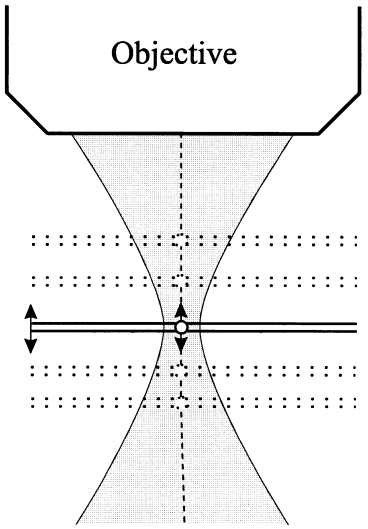

Fig. 1. Measuring the axial response using a thin planar object or a small particle scanned through the focal region. Note that for the small particle no signal contributions are present from the off-optical-axis region.

references is defined as full width at half maximum (FWHM) of the response curve.

The method using small particles is especially applicable when probing small cellular organelles like lysosomes or small labelled sites. It is less suitable for thicker objects. Compared to a plane object the signal from an axially scanned point object drops quicker when moved out of focus because there is no contribution from regions next to the optical axis (Fig. 1). Therefore, when working with larger objects, the resolution determined with a small particle is underestimating the experimental resolution obtained in the sample. It is our goal to determine the resolution of the Raman set-up for samples larger than the beam diameter and thicker than the confocal parameter of high numerical aperture objectives. All biological samples of relevance to our study (cells, chromosomes, eye lens slices) comply with this criterion.

We present here a simple and straightforward approximation for the axial resolution of a confocal microscope, based on Gaussian optics theory, and compare this with results measured on our confocal Raman microscope using a thin planar object.

Theory

The theory of axial confocality is applicable for both Raman microscopy and fluorescence microscopy, but in the discussion we will focus on Raman only.

We assume a confocal microscope in which the sample is illuminated by a laser beam which is directed through the objective under which a focal spot is formed. The TEM_{00} mode output of a laser is a spherical Gaussian beam. In the ideal case of an aberration-free objective with a completely filled entrance aperture, the intensity distribution in the focus can be described by (Haus, 1984):

$$I(r,z) = \frac{I_0}{1+\dfrac{z^2}{Z_r^2}} \exp\left[\left(-2\frac{r^2}{r_0^2}\right)/\left(1+\frac{z^2}{Z_r^2}\right)\right] \qquad (1)$$

where r_0 is the radius where the lateral Gaussian intensity has fallen to $1/e^2 (= 13{\cdot}5\%)$ of the peak value and $Z_r = n\pi {r_0}^2/\lambda$, the Rayleigh range characterizing the Lorentzian profile along the optical axis ($r = 0$).

If an object is moved through the focus under an objective then an image is formed of the Gaussian intensity profile illuminating the object. The position of this image can be calculated from the Gaussian lens formula:

$$\frac{n}{z_0} + \frac{n'}{z_0'} = \frac{n'}{f} \qquad (2)$$

with f the back focal length in the image space, z_0 the distance between the principle plane U and the in-focus object and $z_0{}'$ the distance between the principle plane U' and the image. The refractive indices of thd medium under the objective and in the image space are denoted by n and n', respectively (Fig. 2). If we assume the image to be in air ($n' = 1$) we can write for a displacement z from z_0:

$$\frac{n}{z_0 - z} + \frac{1}{z_0' + z'} = \frac{1}{f}. \qquad (3)$$

Many microscopes are built around the German ISO standard which specifies a tube length of $L = 160$ mm. This means that for a finite image distance objective with a standard eyepiece-lens of 10 mm an image is formed at $L = 150$ mm behind the entrance pupil of the objective. The distance between the principle plane U' of the objective and the image is fixed to $L + L_u$ (Fig. 2). L_u is the distance between principle plane U' of the objective and the plane from which the tubelength is specified. If an infinity-corrected objective is used an image of the object is formed by a tube lens. The distance $L + L_u$ is then the distance between the image and the principle plane of the tube lens. The distance L_u is different for every objective and should be obtained from the manufacturer and is generally of the order of a few centimetres.

Magnification of an object

With the magnification of the objective being $M = z_0{}'/z_0 = (L + L_u)/z_0$ it can be derived from Eq. (2) that the relation between the magnification, the back focal length and the tubelength L is given by

$$M = \frac{L + L_u}{nf} - \frac{1}{n}. \qquad (4)$$

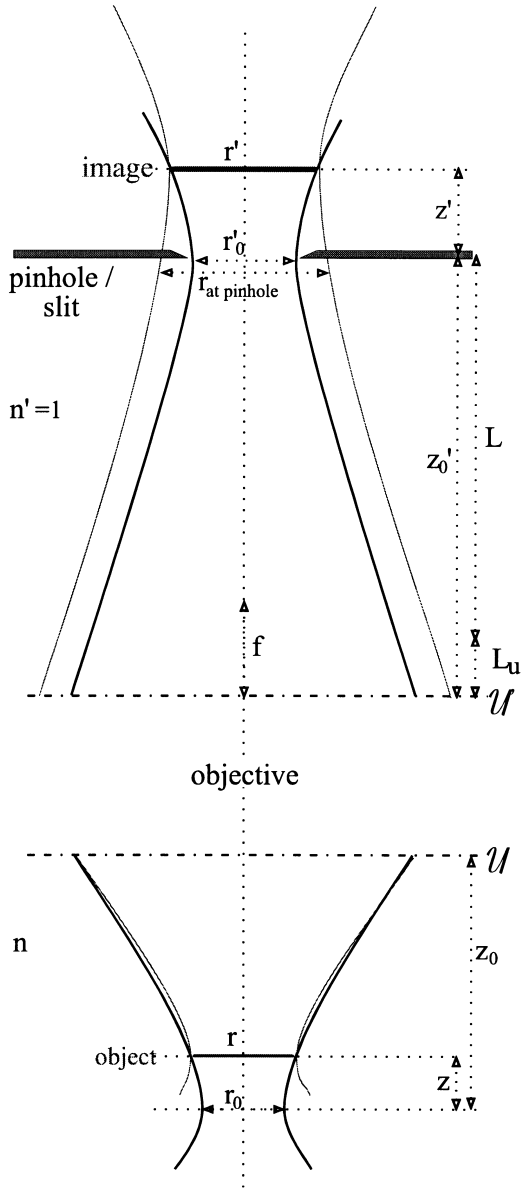

Fig. 2. Scheme showing the symbol definitions as appearing in the formulae. An object at a displacement z from the infocus position z_0 is imaged in the image space at a position $z_0' + z'$. The beam waist at the position of the pinhole/slit of the beam forming the image is $r_{\text{at pinhole}}$. The distances L_u, z_0 and z_0' are measured from the primary and secondary principle plains of the objective lens system which is, for an infinity-corrected objective, the combination of the objective and the tube lens.

This formula is often referred to in a simpler form $M = L/f$ which is valid for large magnification and $n = 1$.

From Eq. (3) we have $z' = (z_0 - z)f/(z_0 - z - nf) - z_0'$ and from Eq. (4) we have the backfocal length: $f = (L + L_u)/(nM + 1)$. The relation between the displacements z and z' then becomes

$$z' = \frac{nM^2(L + L_u)z}{L + L_u - (nM^2 + M)z}. \tag{5}$$

The magnification of an object at a distance z from z_0 is $a = (z_0' + z')/(z_0 - z)$. Using Eq. (5) we find

$$a = \frac{M(L + L_u)}{L + L_u - (nM^2 + M)z}. \tag{6}$$

As can be seen from this formula the magnification is a function of the position z. This implies that the shape of the illuminated object under the objective is not linearly projected into the image space.

Image size of a planar object

For the determination of the axial resolution of a confocal set-up we consider the signal response from a thin plane object that is scanned axially through the focus. In Raman spectroscopy this object is excited with the laser light and becomes a light-emitting object. At a displacement z, the width of the Gaussian beam on the object is given by (Haus, 1984)

$$r = r_0\sqrt{1 + (z/Z_r)^2} \tag{7}$$

where r_0 is the beam waist in focus which should be calculated or derived from experimental results. The size of the image of the illuminating beam is $r' = ar$. The beam forming the image (see Fig. 2) has at the position of the pinhole a waist radius of

$$r_{\text{at\_ph}}(z) = r'\sqrt{1 + (z'/Z_{r\_\text{image}})^2} \tag{8}$$

where Z_{r_image} is the Rayleigh range as calculated from the radius of the object r'.

Intensity throughput through a pinhole

The intensity falling through the pinhole for the object at distance z and thus for a radius $r_{\text{at\_ph}}$ of the beam at the pinhole position is then, from Eq. (1),

$$I_{\text{ph}}(z) = \int_0^{2\pi}\int_0^{R_{\text{ph}}} I'(z, r)\mathrm{d}r\mathrm{d}\phi = \frac{r_0^2}{r'^2} \cdot \frac{2\pi I_0}{1 + \dfrac{z'^2}{Z_{r\_\text{image}}^2}}$$

$$\int_0^{R_{\text{ph}}} \exp\left[\frac{-2r^2}{r'^2}\Big/\left(1 + \frac{z'^2}{Z_{r\_\text{image}}^2}\right)\right].r\mathrm{d}r \tag{9}$$

with R_{ph} the radius of the pinhole. The first factor r_0^2/r'^2 describes the correction for the intensity I_0 for a displacement z. The total intensity under the Gauss curve, being $I_{\text{tot}} = \pi.r_0^2 I_0/2$, should be the same for every position of the image, and therefore I_0 should be corrected with this factor. The second factor arises from the fact that the integral is

evaluated at the pinhole position which is at a distance z' from the image position. Using Eq. (7) and the relation

$$2\pi \int_0^p \exp^{-2\frac{r^2}{w^2}} r\mathrm{d}r = \frac{\pi}{2} w^2 \left(1 - \mathrm{e}^{-2\frac{p^2}{w^2}}\right)$$

we obtain for the intensity throughput through the pinhole:

$$I_{\mathrm{ph}}(z) = \frac{\pi . r_0^2 I_0}{2} \left[1 - \exp\left(\frac{-2R_{\mathrm{ph}}^2}{r_{\mathrm{at\_ph}}^2}\right)\right]. \qquad (10)$$

Intensity throughput through a slit

For a slit the light transmitted is the intensity of the beam at the slit position, integrated over the slit dimensions L_{sl} and R_{sl} giving

$$I_{\mathrm{sl}}(z) = \frac{r_0^2}{r'^2} \cdot \frac{I_0}{1 + \frac{z'^2}{Z_{r\_\mathrm{image}^2}}} \int_{-R_{\mathrm{sl}}}^{R_{\mathrm{sl}}} \int_{-L_{\mathrm{sl}}}^{L_{\mathrm{sl}}} \exp\left(\frac{-2(x^2 + y^2)}{r_{\mathrm{at\_pinh}}{}^2}\right) \mathrm{d}x\mathrm{d}y \qquad (11)$$

To obtain the transmission through the pinhole and the slit, the intensities normalized for the transmission without the pinhole are given by: $T_{\mathrm{pinhole}} = I_{\mathrm{ph}}/I_{\mathrm{tot}}$ and $T_{\mathrm{slit}} = I_{\mathrm{sl}}/I_{\mathrm{tot}}$.

Experimental

Raman measurements were performed on a confocal raman microscope (Puppels *et al.*, 1990). A laser beam of 660 nm from a DCM operated dye laser (Spectra Physics 375B) was focused on to the sample using an objective. A focus before the objective ensures that the entrance pupil of the objective is always completely filled and at the same time allows the insertion of a pinhole or slit for confocality. The back-scattered signal is dispersed using a grating. Subsequently it is focused by a silver-coated concave mirror on to a liquid-nitrogen-cooled CCD camera (backthinned TBK512 Wright Instruments, U.K.). The system is optimized for signal throughput and optical quality using only two (achromat) lenses, one grating (Milton Roy, U.S.A.) and one concave mirror.

For the determination of the axial resolution of the confocal set-up a thin layer of polystyrene was measured. Polystyrene was dissolved in toluene. This solution was spin coated on a quartz substrate and stored for several days. The thickness is 0·16 μm as determined by a Dektak 2A surface profiler. The sample was axially moved through the focus using a motorized, computer-controlled object table. Circular pinholes of 50 μm and 100 μm diameter and a slit of 50 μm width were used in the measurements. Three different microscope objectives were used: (1) a Zeiss, Plan NeoFluar 63×, NA = 1·2 water-immersion objective, (2) a Spindler & Hoyer (S & H) 63×, NA = 0·85 objective and (3) a Nikon 40×, NA = 0·65 objective, all for a finite image distance of 150 mm. For the Zeiss water-immersion objective distilled water ($n = 1{\cdot}33$) was used as a medium between the object and the objective; the S & H and Nikon objectives were corrected for usage in air and used accordingly.

Results

Spectra were recorded from the polystyrene layer at a range of positions under the objective. The integrated intensity of the 1000 cm^{-1} polystyrene vibration, corrected for background signal, was determined and taken as a measure of the signal throughput. For every objective and pinhole/slit combination five series of measurements were done. The averaged results together with the standard deviation are presented in Fig. 3.

The calculations are based on the model for Gaussian beams as given by Eq. (1). It was therefore checked whether the beam under the objective has a Gaussian intensity distribution. The intensity distribution was measured in the far field (12 cm below the objective), for all objectives in air, using a pin detector. The lateral intensity distribution matched a Gaussian profile. The axial distribution, although difficult to measure near to the focal plane, was very well fitted with a Lorentzian profile. For the objectives which are operated in air the diameter of the beam in focus can be calculated from the diameter of the Gaussian distribution in the far field using Eq. (7). For the S & H objective this resulted in a spot radius in focus of $r_0 = 0{\cdot}75$ μm and for the Nikon 40× objective $r_0 = 0{\cdot}9$ μm. For the Zeiss water immersion objective a similar calculation was not possible since we did not perform these measurements in air. For the Zeiss 63× objective it can be calculated that a Gaussian beam, which is not truncated at the objective aperture, results in a Gaussian focal spot with a waist of $r_0 = 0{\cdot}35$ μm. These spot radii were used in calculations of the transmission response according the method described above. For the Zeiss 63×/1·2 objective the value of L_u was 12 mm, for the S & H and the Nikon objectives $L_u = 40$ mm. It should be noted that the calculations show only little dependence on the length of L_u. The calculated responses are shown in Fig. 3. The measured data were scaled with a factor to obtain a maximum transmission corresponding to the calculated

Fig. 3. Response of a thin polystyrene layer under an objective in a confocal microscope. The averaged integrated intensity of the polystyrene band at 1000 cm^{-1} and its standard deviation (+) and the calculated response (—) are shown: for a 63×/1·2NA water-immersion objective and a pinhole diameter of 50 μm (A), 100 μm (B) and a slit of 50 μm width (C); for a 63×/0·85NA objective in air and a pinhole diameter of 50 μm (D) and 100 μm (E); for a 40×/0·65NA objective in air and a pinhole diameter of 50 μm (F) and 100 μm (G).

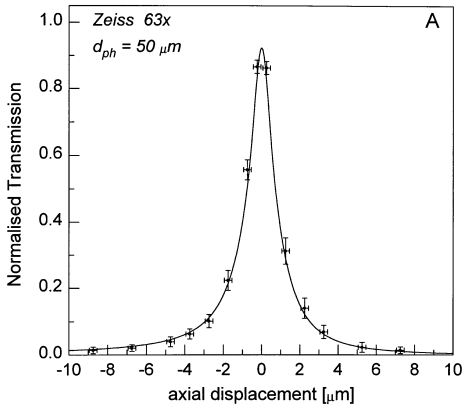
Zeiss 63x
d_{ph} = 50 μm
A
Normalised Transmission
axial displacement [μm]

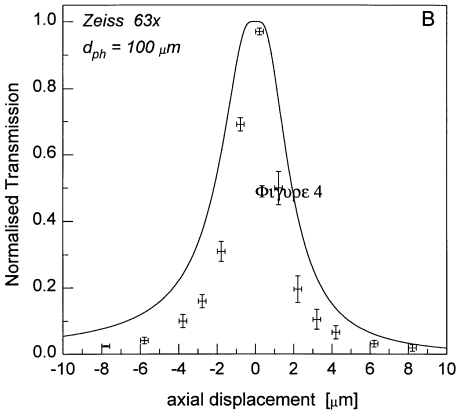
Zeiss 63x
d_{ph} = 100 μm
B
Normalised Transmission
axial displacement [μm]

Φιγυρε 4

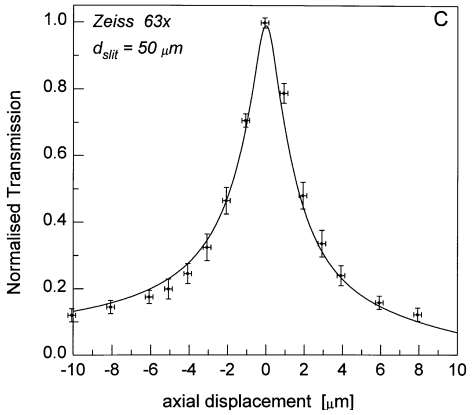
Zeiss 63x
d_{slit} = 50 μm
C
Normalised Transmission
axial displacement [μm]

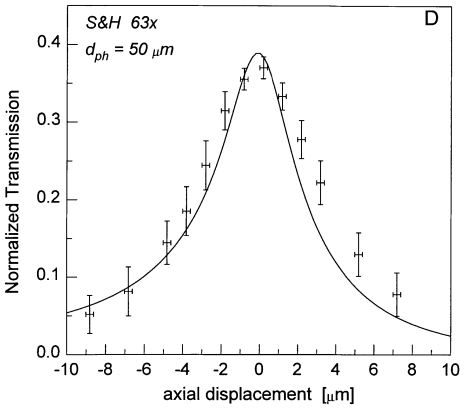
S&H 63x
d_{ph} = 50 μm
D
Normalized Transmission
axial displacement [μm]

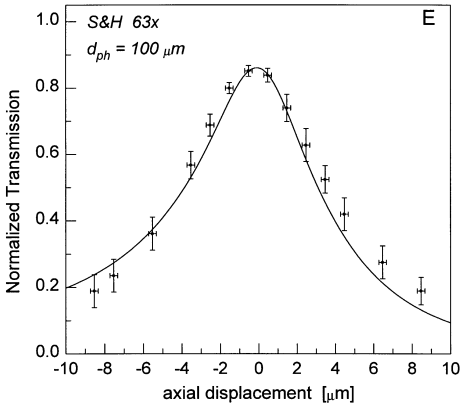
S&H 63x
d_{ph} = 100 μm
E
Normalized Transmission
axial displacement [μm]

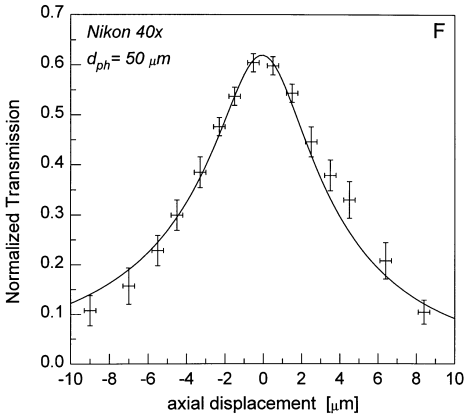
Nikon 40x
d_{ph}= 50 μm
F
Normalized Transmission
axial displacement [μm]

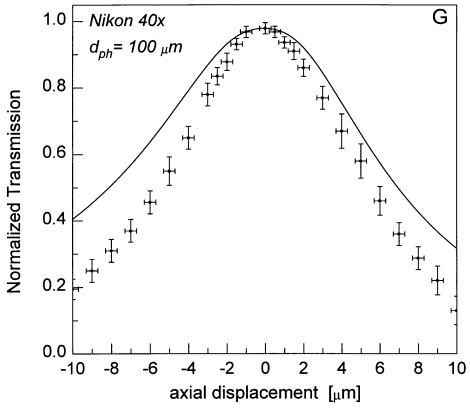
Nikon 40x
d_{ph}= 100 μm
G
Normalized Transmission
axial displacement [μm]

Table 1. FWHM (μm) of measured and calculated response curves.

	50-μm pinhole	100-μm pinhole	50-μm slit
Measured			
Zeiss 63×/1·2	1·7 ± 0·4	2·4 ± 0·3	3·5 ± 0·4
S & H 63×/0·85	7·1 ± 1·2	8·9 ± 1·5	
Nikon 40×/0·65	9·3 ± 1·5	11·3 ± 1·2	
Calculated			
Zeiss 63×/1·2	1·7	4·1	3·5
S & H 63×/0·85	5·5	8·8	
Nikon 40×/0·65	8·5	15·4	

curve. All calculations were performed on a PC (486DX) and use negligible computation time.

The measured and calculated axial resolutions (FWHM) are listed in Table 1.

In Fig. 4 the FWHM calculated with the Gaussian model for a diffraction-limited spot is plotted as a function of pinhole size. The curve was calculated for the case of the Zeiss 63×/1·2 objective with $r_0 = 0{\cdot}35\,\mu$m. For comparison the curve as calculated with electromagnetic diffraction theory is plotted for the same objective. This curve was calculated according the model described in Wilson & Tan (1995) and results in a curve which is nearly identical to that given by van der Voort & Brakenhoff (1990). This model calculates the axial resolution for a high numerical objective illuminated with a uniform plane wavefront. It is not therefore directly comparable with the case of a Gaussian illuminated object.

Discussion

Gaussian beam theory is valid only for the paraxial case where the propagation direction of the light is under a small angle with the optical axis. In a plane above the focus the rays at a distance from the optical axis enter under a larger angle (Fig. 5). For a larger pinhole, a larger part of these rays pass through the pinhole. In this case, when out of focus, Gaussian calculation will give a deviation from the intensity measured. In the true confocal case the light passing through the pinhole comes from a volume which is much more confined to the optical axis. This effect therefore will only arise for an objective–pinhole combination that is not confocal.

For a confocal objective–pinhole combination the pinhole should be smaller than the diameter of the in focus spot which is falling on the pinhole. In terms of the model $r_0' = Mr_0r_{ph}$. The radius of r_0' for the Zeiss 63×, S & H 63× and Nikon 40× objectives is 22, 94 and 72 μm, respectively. This implies that for the Zeiss 63× objective and the Nikon

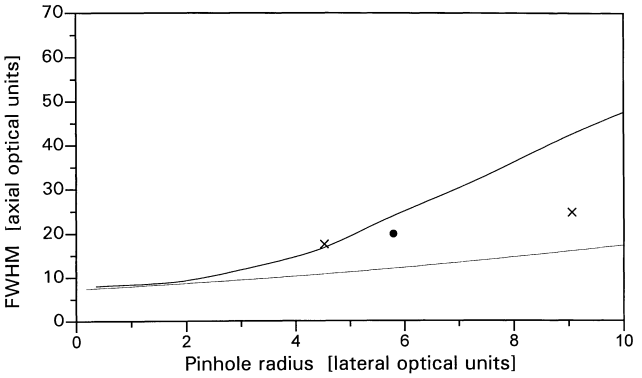

Fig. 4. Calculated axial resolution (FWHM) as a function of the pinhole radius for a thin plane object. Thick line: calculated with the Gaussian model, where the object is illuminated with the Gaussian laser spot. Thin line: calculated electromagnetic diffraction theory model (Wilson & Tan, 1995) for a planar uniform light-emitting object. (x) Measured with the Zeiss 63×/1·2NA water-immersion objective. (●) Measured by Markwort *et al.* (1995) using a 100×/0·95NA objective. Axes are given in optical units under the objective defined by $u = z.kNA^2/n$ and $v_{ph} = r_{ph}.kNA/M$, with $k = 2\pi/\lambda$ and M the magnification of the objective.

40× objective in combination with a pinhole radius of 100 μm the set-up is not confocal. This can be observed from the calculated responses in Fig. 3. It is especially apparent in the flat top in Fig. 3(B). For a distance of about 1 μm from the focal plane all the calculated intensity from the focus is falling through the pinhole indicating that in this area the focal radius is smaller than the pinhole. The Rayleigh range (Z_r) gives a measure of the length of the

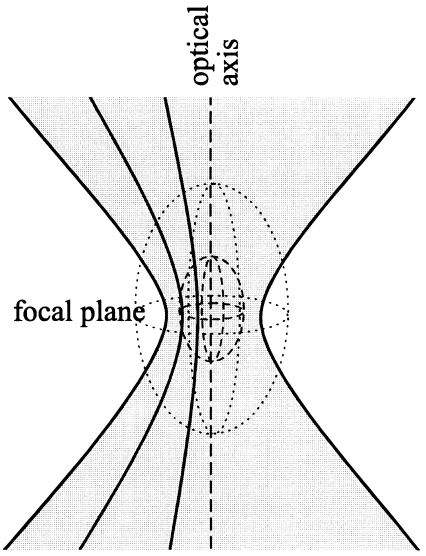

Fig. 5. Focal region under the objective. The measuring volumes for two pinhole sizes, in the confocal (small volume) and the nonconfocal cases (large volume), are depicted.

focus. For the Zeiss objective the value for the Rayleigh range is $Z_r = 0{\cdot}58\,\mu$m. This explains why for an object just out of focus ($z > 0{\cdot}58\,\mu$m) the calculated intensity is higher than measured.

Comparing the calculated curve, using the Gaussian model, in Fig. 3 with those predicted by models using point spread function calculations based on electromagnetic diffraction theory (van der Voort & Brakenhoff, 1990; Wilson & Tan, 1995), the model described here gives, in the confocal region, a similar curve. The electromagnetic diffraction models start with a uniform planar object wavefront, while the model presented here has a Gaussian object. The curve of the Gaussian model therefore depends on object waist. In the case of the Zeiss 63×/1·2 objective, with a diffraction-limited spot of r_0 of $0{\cdot}35\,\mu$m, the offset of both curves is identical. The slope of the Gaussian curve, for larger pinhole sizes, is larger than that expected from the measurements. This phenomenon is ascribed to the non-confocal geometry, which is not described correctly with the Gaussian model.

For a 50-μm pinhole and the Zeiss 63×/1·2 objective an axial resolution of $1{\cdot}7\,\mu$m is obtained. This is of the order of the $1{\cdot}8\,\mu$m which was determined with a 100×/0·95 objective, a 100-μm pinhole and 514·5-nm laser excitation (Markwort *et al.*, 1995). The axial resolution determined here using a plane object is, as expected, larger than the $1{\cdot}3\,\mu$m measured with small beads under the same conditions (Puppels *et al.*, 1991). For an infinitely thin planar fluorescent object and a 50-μm slit an axial resolution of $2\,\mu$m (for the 63×/1·2 objective and 660-nm light) can be obtained from Wilson (1990) We were not able to obtain this resolution experimentally.

For the confocal case of the set-up, for the pinholes as well as for the slit, the Gaussian model results in a response that fits well to the measured data. We conclude that Gaussian beam theory provides an appealing model that is easy to use. It provides a quick prediction of the axial resolution of a confocal microscope in the true confocal case.

References

Brakenhoff, G.J., van der Voort, H.T.M., van Spronsen, E.A. & Nanninga, N. (1986) Three-dimensional imaging by confocal scanning fluorescence microscopy. *Ann. NY Acad. Sci.* **483,** 405–415.

Duindam, H.J., Vrensen, G.F.J.M., Otto, C., Puppels, G.J. & Greve, J. (1995) New approach to assess the cholesterol distribution in the eye lens: confocal Raman microspectroscopy and filipin cytochemistry. *J. Lipid Res.* **36,** 1139–1146.

Haus, H.A. (1984) *Waves and Fields in Optoelectronics*. Prentice-Hall, London.

Markwort, L., Kip, B., Da Silva, E. & Roussel, B. (1995) Raman Imaging of heterogeneous polymers: a comparison of global versus point illumination. *Appl. Spectrosc.* **49,** 1411–1429.

Puppels, G.J., Bakker Schut, T.C., Sijtsema, N.M., Grond, M., Maraboeuf, F., Grauw, C.J., Figdor, C.G. & Greve, J. (1995) Development and application of Raman microspectroscopic and Raman imaging techniques for cell biological studies. *J. Mol. Struct.* **374,** 477–484.

Puppels, G.J., Colier, W., Olminkhof, J.H.F., Otto, C., de Mul, F.F.M., Greve, J. (1991) Description and performance of a highly sensitive confocal Raman microscope. *J. Raman Spectrosc.* **22,** 217–225.

Puppels, G.J., de Mul, F.F.M., Otto, C., Greve, J., Robert-Nicoud, M., Arndt-Jovin, D.J. & Jovin, T.M. (1990) Studying single living cells and chromosomes by confocal raman microscopy. *Nature*, **347,** 301–303.

Sharonov, S., Nabiev, I., Choura, I., Feafanov, A., Valisa, P. & Manfait, M. (1994) Confocal three-dimensional scanning laser Raman-SERS-fluorescence microprobe. Spectral imaging and High-resolution applications. *J. Raman Spectrosc.* **25,** 699–707.

van vander Voort, H.T.M. & Brakenhoff, G.J. (1990) 3-D image formation in high-aperture fluorescence confocal microscopy: a numerical analysis. *J. Microsc.* **158,** 43–54.

Wilson, T. (1990) *Confocal Microscopy.* Academic Press, London.

Wilson, T. & Carlini, A.R. (1987) Size of the detector in confocal imaging systems. *Opt. Lett.* **12,** 227–229.

Wilson, T. & Hewlett, S.J. (1990) Imaging in scanning microscopes with slit-shaped detectors. *J. Microsc.* **160,** 115–139, and references therein.

Wilson, T. & Tan, J.B. (1995) Finite sized coherent and incoherent detectors in confocal microscopy. *J. Microsc.* **182,** 61–66.